Journal of Solid State Chemistry **155,** 417–426 (2000)
doi:10.1006/jssc.2000.8944, available online at http://www.idealibrary.com on IDEAL®

$Rb_{2n}(Mo_9S_{11})(Mo_{6n}S_{6n+2})$ ($n = 1$ to 4): A Novel Family of Superconducting Molybdenum Cluster Compounds

Soazig Picard, Jean-Yves Saillard, Patrick Gougeon,[1] Henri Noël, and Michel Potel

Laboratoire de Chimie du Solide et Inorganique Moléculaire, UMR CNRS 6511, Université de Rennes 1, Avenue du Général Leclerc, 35042 Rennes-Cedex, France

Received June 6, 2000; in revised form July 25, 2000; accepted August 17, 2000; published online November 29, 2000

Reinvestigation of the Rb–Mo–S system has led to the discovery of a novel family of reduced molybdenum sulfides with the general formula $Rb_{2n}(Mo_9S_{11})(Mo_{6n}S_{6n+2})$ ($n = 1$ to 4) in addition to the previously known compound $Rb_2Mo_6S_6$. The new rubidium-reduced molybdenum sulfides have been prepared by solid-state reaction of Rb_2MoS_4, MoS_2, and Mo heated at temperatures ranging between 1600 K and 2000 K in a sealed Mo crucible. All members of the family crystallize in the *R*-3*c* space group with $Z = 6$ in the hexagonal setting. X-ray diffraction studies on single crystals showed that their crystal structures consist of an equal mixture of Mo_9S_{11} and $Mo_{6n}S_{6n+2}$ ($n = 1$ to 4) cluster units interconnected through Mo–S bonds. The Rb^+ cations occupy large voids between the different cluster units. When *n* goes from 1 to 4, the *a* parameter of the hexagonal unit cell decreases from 9.433(1) Å to 9.237(1) Å, whereas the *c* parameter increases linearly from 56.27(1) Å to 137.28(2) Å. Extended Hückel (tight-binding) calculations revealed that the clusters are hypoelectronic and the Fermi level crosses a rather flat band for all members of the family. Resistivity measurements carried out on single crystals from 290 K to 2 K confirmed the metallic behavior and each member was found to be a superconductor with transition temperatures ranging from 4.2 K to 10.9 K.
© 2000 Academic Press

INTRODUCTION

The first example of a molybdenum cluster with nuclearity higher than six was the bioctahedral Mo_9 species observed in the ternary compounds $In_3Mo_{15}Se_{19}$ (1) and $In_2Mo_{15}Se_{19}$ (2) two decades ago. In the latter two compounds, the Mo_9 cluster, which results from the metal face-sharing of two Mo_6 octahedra, coexists with the Mo_6 cluster in equal proportions. A short time later, the Mo_{12} cluster (i.e., three face-shared Mo_6 octahedra) was also found with the monomeric Mo_6 cluster in the ratio 1:1 in the $Tl_2Mo_9S_{11}$ compound (3). Subsequently, both condensed clusters as well as clusters of higher nuclearity, namely Mo_{15}, Mo_{18}, Mo_{21}, Mo_{24}, Mo_{30}, and Mo_{36}, were found to be present in the series of compounds $M_{n-2}Mo_{3n}X_{3n+2}$ (M = Rb, Cs; X = S, Se, or Te; $n = 3, 4, 5, 6, 7, 8, 10$, and 12) (4–10). The members with even n crystallize in the rhombohedral trigonal space group *R*-3 with a structure closely related to that of the ternary chalcogenides MMo_6X_8 (11) and the members with odd n crystallize in the hexagonal space group $P6_3/m$. The ending member, which also crystallizes in the space group $P6_3/m$, corresponds to the one-dimensional compound $M_2Mo_6X_6$ containing infinite chains of trans-face-sharing Mo_6 octahedra $|Mo_{6/2}|^1_\infty$ (12, 13). The interest in these compounds lies not only in their fascinating structural aspects but also in their interesting physical properties. Indeed, the sulfides and selenides generally present superconducting or metal–insulator transitions at low temperature. Thus, studies of the normal and superconducting states of both $Cs_2Mo_{12}Se_{14}$ ($n = 4$) and $Rb_4Mo_{18}Se_{20}$ ($n = 6$) by measuring the conductivity and magnetization of single crystals and powder samples have shown that these compounds can be classified among the "exotic" superconductors (14). The quasi-1-D superconductor $Tl_2Mo_6Se_6$ presents extreme type II and non-BCS behaviors (15–18). In addition, the anisotropy of the electronic properties in the latter compound is one of the largest ever observed in a superconductor with the ratio of the conductivities parallel and perpendicular to the infinite chains ($\sigma_{//}/\sigma_{\perp}$) about 1000, and the ratio of the upper critical fields ($Hc_{2//}/Hc_{2\perp}$) about 26.

We report here on the syntheses, structural, and theoretical studies along with physical properties of a new family of superconducting compounds containing two different cluster types. Indeed, this family is characterized by an equal mixture of odd-membered Mo_9S_{11} and even-membered $Mo_{6n}S_{6n+2}$ ($n = 1$ to 4) cluster units.

[1] To whom correspondence should be addressed. Fax: (33) 2.99.63.57.04. E-mail: Patrick.Gougeon@univ-rennes1.fr.

0022-4596/00 $35.00
Copyright © 2000 by Academic Press
All rights of reproduction in any form reserved.

EXPERIMENTAL

Synthesis. Starting materials used for the syntheses were MoS_2, Rb_2MoS_4, and Mo, all in powder form. Before use, Mo powder (Plansee 99.99%) was reduced under H_2 flux at 1000°C for 10 hours in order to eliminate any trace of oxygen. The molybdenum disulfide was prepared by the reaction of sulfur (Fluka 99.999%) with H_2-reduced Mo in a ratio of 2:1 in an evacuated (ca. 1 Pa Ar residual pressure) and sealed silica tube, heated at 800°C for 2 days. The rubidium thiomolybdate was obtained by sulfuration of Rb_2MoO_4 at 450°C for 2 days under a CS_2 gas carried out by flowing argon. The molybdate Rb_2MoO_4 was synthesized by heating an equimolar ratio of MoO_3 (CERAC 99.95%) and Rb_2CO_3 (CERAC 99.9%) in an alumina vessel at 800°C in air over 2 days. The purity of all starting reagents was checked by powder X-ray diffraction on an Inel curve-sensitive position detector CPS 120. Furthermore, in order to avoid any contamination by oxygen and moisture, the starting reagents were kept and handled in a purified argon-filled glove box.

Single-phase powder samples of the $Rb_{2n}(Mo_9S_{11})(Mo_{6n}S_{6n+2})$ series were synthesized from stoichiometric mixtures of MoS_2, Rb_2MoS_4, and Mo. The starting materials were mixed, ground together, and then cold-pressed. The pellet (ca. 5 g) was then loaded in a molybdenum crucible which was sealed under low argon pressure using an arc welding system. The crucible was heated at a rate of 300°C h^{-1} to 1500°C and held there for 48 hours, and then cooled at 100°C h^{-1} to 1100°C and finally furnace cooled to room temperature. The purity of all products was checked by powder X-ray diffraction. To obtain single crystals of quality and size suitable for X-ray diffraction and resistivity measurements, an excess of Rb_2MoS_4 of 5% in weight was necessary.

X-ray diffraction and structure determination. Single crystals of each compound was selected and mounted on a glass fiber. They were investigated by X-ray diffraction by the ω–2θ scan method on a Nonius CAD-4 diffractometer equipped with graphite-monochromatized Mo$K\alpha$ radiation ($\lambda = 0.71073$ Å) at room temperature. Lattice parameters were obtained by least-squares refinement of the setting angles of 25 reflections. The absorption correction was done empirically using the Ψ-scan method (19) on the $Rb_4Mo_{21}S_{25}$, $Rb_6Mo_{27}S_{31}$, and $Rb_8Mo_{33}S_{37}$ data sets.

The four structures were solved by direct methods in the trigonal space group R-3c using the Molen package (20) and subsequently refined by full least-squares methods on F using the JANA98 program (21). The refinement converged to $R = 0.0387$, $R_w = 0.0421$; $R = 0.0305$, $R_w = 0.0286$;

TABLE 1
X-Ray Crystallographic and Experimental Data of $Rb_{2n}(Mo_9S_{11})(Mo_{6n}S_{6n+2})$ ($n = 1$ to 4)

Formula	$Rb_2Mo_{15}S_{19}$	$Rb_4Mo_{21}S_{25}$	$Rb_6Mo_{27}S_{31}$	$Rb_8Mo_{33}S_{37}$
n	1	2	3	4
FW, g.mol^{-1}	2219.2	3148.1	4097	5036
Space group	R-3c (No. 167)	R-3c (No. 167)	R-3c (No. 167)	R-3c (No. 167)
a_h, Å	9.4326(8)	9.3352(6)	9.2801(5)	9.2372(7)
c_h, Å	56.27(1)	83.64(1)	110.50(2)	137.28(2)
Z_h			6	
V_h, Å^3	4336(1)	6312.4(9)	8241(2)	10144(2)
l_{rh}, Å	19.533(2)	28.395(2)	37.220(3)	46.070(3)
α_{rh}, °	27.945(3)	18.922(1)	14.3229(9)	11.5074(5)
Z_{rh}			2	
V_{rh}, Å^3	1445.4(2)	2104.0(3)	2747.0(3)	3381.5(3)
ρ_{calc}, g cm^{-3}	5.097	4.967	4.949	4.944
T, °C			20	
λ, Å			0.71073 (Mo$K\alpha$)	
Crystal dimens., mm^3	$0.1 \times 0.08 \times 0.08$	$0.16 \times 0.16 \times 0.13$	$0.1 \times 0.08 \times 0.08$	$0.16 \times 0.05 \times 0.02$
Scanning mode			ω–2θ	
θ_{max}	30	35	35	30
Measured reflns	3057	3817	4224	3888
Unique reflns ($I/\sigma(I) > 3$)	758	2117	2493	1142
R_{int}	0.029	0.018	0.041	0.041
Refined parameters	57	78	99	120
S = goodness of fit	1.18	1.47	1.64	0.77
μ, mm^{-1}	10.974	11.853	12.383	12.745
R_1[a] ($I/\sigma(I) > 3$)	0.0387	0.0305	0.0323	0.0250
wR_2[b] ($I/\sigma(I) > 3$)	0.0421	0.0286	0.0307	0.0228

[a] $R_1 = \sum \| F_o| - |F_c \| / \sum |F_o|$. [b] $wR_2 = \{\sum [w(F_o - F_c)^2] / \sum [w(F_o)^2]\}^{1/2}$, $w = 1/[\sigma^2(F_o) + 0.0001]$.

TABLE 2

Atomic Coordinates and Equivalent Isotropic Displacement Parameters (Å^2) for 1 ($Rb_2Mo_{15}S_{19}$), 2 ($Rb_4Mo_{21}S_{25}$), 3 ($Rb_6Mo_{27}S_{31}$), and 4($Rb_8Mo_{33}S_{37}$)

Atom	Site	τ	x	y	z	U(eq)
			1, $Rb_2Mo_{15}S_{19}$			
Mo(1)	36*f*	1	0.1598(1)	− 0.0082(1)	0.20959(1)	0.0076(4)
Mo(2)	18*e*	1	0.8355(2)	0	0.25	0.0078(4)
Mo(3)	36*f*	1	0.1724(1)	0.0188(1)	0.02040(2)	0.0084(4)
S(1)	36*f*	1	0.7122(3)	0.0189(3)	0.21381(5)	0.011(1)
S(2)	18*e*	1	0.3021(4)	0	0.25	0.010(1)
S(3)	36*f*	1	0.3509(3)	0.2985(3)	0.34969(5)	0.009(1)
S(t1)	12*c*	1	0	0	0.21267(2)	0.0088(6)
S(t2)	12*c*	1	0	0	0.05356(9)	0.015(1)
Rb(1)	12*c*	1	0	0	0.11324(4)	0.0235(6)
			2, $Rb_4Mo_{21}S_{25}$			
Mo(1)	36*f*	1	0.16147(4)	0.99203(4)	0.222752(3)	0.0064(1)
Mo(2)	18*e*	1	0.83399(5)	0	0.25	0.0060(1)
Mo(3)	36*f*	1	0.15115(4)	0.97846(4)	0.459881(3)	0.0065(1)
Mo(4)	36*f*	1	0.98302(4)	0.82599(4)	0.487102(3)	0.0061(1)
S(1)	36*f*	1	0.3089(1)	0.2911(1)	0.22549(1)	0.0086(3)
S(2)	18*e*	1	0.3050(1)	0	0.25	0.0098(4)
S(3)	36*f*	1	0.2849(1)	0.3244(1)	0.03769(1)	0.0085(3)
S(4)	36*f*	1	0.6974(1)	0.0441(1)	0.31972(1)	0.0095(3)
S(t1)	12*c*	1	0	0	0.20064(2)	0.0102(4)
S(t2)	12*c*	1	0	0	0.06227(2)	0.0098(4)
Rb(1)	12*c*	1	0	0	0.100964(9)	0.0195(2)
Rb(2)	12*c*	1	0	0	0.15969(1)	0.0266(2)
			3, $Rb_6Mo_{27}S_{31}$			
Mo(1)	36*f*	1	0.82865(6)	− 0.49697(6)	0.062711(4)	0.0065(2)
Mo(2)	18*e*	1	0.16703(8)	0	0.25	0.0065(2)
Mo(3)	36*f*	1	0.97776(6)	− 0.84899(6)	0.050254(4)	0.0069(2)
Mo(4)	36*f*	1	0.01757(6)	− 0.15704(6)	0.029769(4)	0.0066(2)
Mo(5)	36*f*	1	0.98119(6)	0.15564(6)	0.010089(4)	0.0065(2)
S(1)	36*f*	1	0.0178(2)	0.7074(2)	0.26857(1)	0.0083(5)
S(2)	18*e*	1	0	0.3066(2)	0.25	0.0093(6)
S(3)	36*f*	1	0.0423(2)	− 0.2854(2)	0.04863(1)	0.0094(5)
S(4)	36*f*	1	0.0435(2)	0.6995(2)	0.19687(1)	0.0095(5)
S(5)	36*f*	1	0.0364(2)	0.3266(2)	0.50985(1)	0.0101(5)
S(t1)	12*c*	1	0	0	0.21267(2)	0.0088(6)
S(t2)	12*c*	1	0	0	0.06700(2)	0.0098(6)
Rb(1)	12*c*	1	0	0	0.09609(1)	0.0193(3)
Rb(2)	12*c*	1	0	0	0.13771(1)	0.0327(4)
Rb(3)	12*c*	1	0	0	0.18160(1)	0.0260(3)
			4, $Rb_8Mo_{33}S_{37}$			
Mo(1)	36*f*	1	− 0.1707(2)	− 0.4963(1)	0.066710(9)	0.0071(4)
Mo(2)	18*e*	1	0.8322(2)	0	0.25	0.0075(5)
Mo(3)	36*f*	1	0.1742(2)	0.0229(2)	0.056504(8)	0.0080(5)
Mo(4)	36*f*	1	0.0187(2)	− 0.1570(2)	0.040078(7)	0.0074(5)
Mo(5)	36*f*	1	0.1759(2)	0.0211(2)	0.024181(7)	0.0073(5)
Mo(6)	36*f*	1	0.0215(2)	− 0.1544(2)	0.007957(8)	0.0075(5)
S(1)	36*f*	1	− 0.0218(4)	− 0.6491(5)	0.06836(3)	0.011(1)
S(2)	18*e*	1	0.3083(5)	0	0.25	0.012(2)
S(3)	36*f*	1	0.0438(4)	− 0.2853(4)	0.05525(2)	0.010(1)
S(4)	36*f*	1	0.3254(4)	0.0348(5)	0.04035(2)	0.010(1)
S(5)	36*f*	1	0.0413(5)	− 0.2894(5)	0.02400(2)	0.011(2)
S(6)	36*f*	1	0.3300(5)	0.0424(5)	0.00808(2)	0.011(2)
S(t1)	12*c*	1	− 0.333333	− 0.666667	0.05324(4)	0.009(1)
S(t2)	12*c*	1	0	0	0.06999(4)	0.012(2)
Rb(1)	12*c*	1	0	0	0.09337(2)	0.0199(7)
Rb(2)	12*c*	1	0	0	0.12633(2)	0.0293(9)
Rb(3)	12*c*	1	0	0	0.15938(2)	0.033(1)
Rb(4)	12*c*	1	0	0	0.19469(2)	0.0250(8)

[a] U(eq) is defined as one-third of the trace of the orthogonalized U_{ij} tensor. τ is the site occupancy.

$R = 0.0323$, $R_w = 0.0307$; and $R = 0.0250$, $R_w = 0.0228$ for $Rb_2Mo_{15}S_{19}$, $Rb_4Mo_{21}S_{25}$, $Rb_6Mo_{27}S_{31}$, and $Rb_8Mo_{33}S_{37}$, respectively. The highest residual electron density peak has a height of 1.80, 2.18, 3.03, and 4.08 for $Rb_2Mo_{15}S_{19}$, $Rb_4Mo_{21}S_{25}$, $Rb_6Mo_{27}S_{31}$, and $Rb_8Mo_{33}S_{37}$, respectively. The crystallographic data as well as details of the structure analysis of each compound are given in Table 1. The final atomic coordinates and equivalent isotropic displacement parameters are reported in Table 2 and selected interatomic distances in Table 3.

Electrical conductivity and magnetic susceptibility measurements. Resistivity measurements were carried out on single crystals for the four members of the family using a conventional ac four-probe method. Contacts were ultrasonically made with molten indium, on single crystals previously characterized on a CAD-4 diffractometer. For the current use (0.1 mA), we checked that a good ohmic behavior was obtained and that no shift of the phase was observed at 90° at low and room temperatures. The magnetic susceptibility data of cold-pressed pellets (ca. 150 mg) were recorded using a SQUID magnetometer SHE in the temperature range 1–20 K with an applied field of 10 G.

Extended Hückel calculations. Molecular (22) and tight-binding (23) calculations were carried out using the programs CACAO (24) and YaEHMOP (25), respectively. The X-ray crystal structures of $Rb_2Mo_{15}S_{19}$, $Rb_4Mo_{21}S_{25}$, $Rb_6Mo_{27}S_{31}$, and $Rb_8Mo_{33}S_{37}$ were considered in the calculations. The exponents (ζ) and the valence shell ionization potentials (H_{ii} in eV) were (respectively) 1.817, − 20.0 for S 3*s*; 1.817, − 13.3 for S 3*p*; 1.956, − 8.34 for Mo 5*s*; 1.921, − 5.24 for Mo 5*p*; 0.997, − 4.18 for Rb 5*s*; and 0.997, − 2.60 for Rb 5*p*. The H_{ii} value for Mo 4*d* was set equal to − 10.50. A linear combination of two Slater-type orbitals of exponents $\zeta_1 = 4.542$ and $\zeta_2 = 1.901$ with equal weighting coefficients was used to represent the Mo 4*d* atomic orbitals. The density of states for each calculated compound was obtained using a set of 8k points.

TABLE 3
Selected Interatomic Distances

	$Rb_2Mo_{15}S_{19}$	$Rb_4Mo_{21}S_{25}$	$Rb_6Mo_{27}S_{31}$	$Rb_8Mo_{33}S_{37}$
		Mo_9 Intratriangle		
Mo(1)–Mo(1) (× 2)	2.680(2)	2.6775(7)	2.6678(7)	2.666(2)
Mo(2)–Mo(2) (× 2)	2.688(3)	2.6841(6)	2.6848(9)	2.685(3)
		Mo_{6n} Intratriangle		
Mo(3)–Mo(3) (× 2)	2.676(2)	2.6354(7)	2.6243(9)	2.623(4)
Mo(4)–Mo(4) (× 2)		2.6868(7)	2.6766(9)	2.674(3)
Mo(5)–Mo(5) (× 2)			2.6658(9)	2.662(2)
Mo(6)–Mo(6) (× 2)				2.660(2)
		Mo_9 Intertriangle		
Mo(1)–Mo(2) (× 2)	2.719(1)	2.7238(3)	2.7232(5)	2.726(2)
Mo(1)–Mo(2) (× 2)	2.785(2)	2.7864(4)	2.7837(6)	2.786(2)
		Mo_{6n} Intertriangle		
Mo(3)–Mo(4)		2.7275(4)	2.7127(6)	2.707(2)
Mo(3)–Mo(4)		2.7663(5)	2.7524(7)	2.743(2)
Mo(4)–Mo(5)			2.6607(7)	2.661(2)
Mo(4)–Mo(5)			2.6713(6)	2.681(2)
Mo(5)–Mo(6)				2.704(1)
Mo(5)–Mo(6)				2.707(2)
Mo(3)–Mo(3)	2.767(2)			
Mo(4)–Mo(4)		2.6573(4)		
Mo(5)–Mo(5)			2.7093(6)	
Mo(6)–Mo(6)				2.6702(9)
		Intercluster		
Mo(1)–Mo(3)	3.246(2)	3.2271(6)	3.223(1)	3.212(3)
		Intratriangle Mo_9		
Mo(1)–S(1)	2.430(3)	2.4287(9)	2.424(3)	2.424(5)
Mo(1)–S(1)	2.466(3)	2.4585(8)	2.457(3)	2.455(6)
Mo(2)–S(2) (× 2)	2.471(3)	2.4690(8)	2.467(2)	2.469(4)
		Intratriangle Mo_{6n}		
Mo(3)–S(3)	2.462(4)	2.4840(8)	2.488(2)	2.481(5)
Mo(3)–S(3)	2.466(3)	2.4928(8)	2.490(2)	2.486(7)
Mo(4)–S(4)		2.473(2)	2.473(2)	2.478(5)
Mo(4)–S(4)		2.4780(9)	2.477(2)	2.479(4)
Mo(5)–S(5)			2.488(2)	2.4912(9)
Mo(5)–S(5)			2.499(2)	2.506(5)
Mo(6)–S(6)				2.481(2)
Mo(6)–S(6)				2.499(2)
		Intertriangle Mo_9		
Mo(1)–S(2) (× 2)	2.622(2)	2.6259(6)	2.6273(8)	2.632(4)
Mo(2)–S(1) (× 2)	2.396(3)	2.4058(9)	2.406(1)	2.408(5)
Mo(1)–S(t1) (× 2)	2.419(4)	2.410(1)	2.404(2)	2.406(4)
		Intertriangle Mo_{6n}		
Mo(3)–S(4) (× 2)		2.587(1)	2.590(1)	2.594(4)
Mo(4)–S(3) (× 2)		2.453(1)	2.468(2)	2.464(5)
Mo(4)–S(5) (× 2)			2.573(2)	2.582(2)
Mo(5)–S(4) (× 2)			2.583(1)	2.584(4)
Mo(5)–S(6) (× 2)				2.583(5)
Mo(6)–S(5) (× 2)				2.582(2)
Mo(3)–S(3) (× 2)	2.434(3)			
Mo(4)–S(4) (× 2)		2.572(1)		
Mo(5)–S(5) (× 2)			2.578(2)	
Mo(6)–S(6) (× 2)				2.576(5)
Mo(3)–S(t2) (× 2)	2.423(4)	2.397(1)	2.392(2)	2.392(4)

TABLE 3—*Continued*

	$Rb_2Mo_{15}S_{19}$	$Rb_4Mo_{21}S_{25}$	$Rb_6Mo_{27}S_{31}$	$Rb_8Mo_{33}S_{37}$
		Intercluster		
Mo(1)–S(3)	2.506(3)	2.506(1)	2.512(1)	2.517(4)
Mo(3)–S(1)	2.433(4)	2.446(1)	2.456(2)	2.456(5)
	Cationic Environment in **1** ($Rb_2Mo_{15}S_{19}$), **2** ($Rb_4Mo_{21}S_{25}$), **3** ($Rb_6Mo_{27}S_{31}$), and **4** ($Rb_8Mo_{33}S_{37}$)			
		1 ($Rb_2Mo_{15}S_{19}$)		
Rb(1)–S(1) (× 3)	3.222(3)			
Rb(1)–S(2) (× 3)	3.706(2)			
Rb(1)–S(3) (× 3)	3.730(3)			
Rb(1)–S(t2)	3.358(6)			
Rb(1)–S(t1)	3.562(5)			
		2 ($Rb_4Mo_{21}S_{25}$)		
Rb(1)–S(1) (× 3)	3.213(1)	Rb(2)–S(3) (× 3)		3.9456(12)
Rb(1)–S(2) (× 3)	3.5708(6)	Rb(2)–S(4) (× 3)		3.5069(7)
Rb(1)–S(3) (× 3)	3.803(1)	Rb(2)–S(4) (× 3)		3.504(1)
Rb(1)–S(t2)	3.236(2)	Rb(2)–S(t1)		3.426(2)
		3 ($Rb_6Mo_{27}S_{31}$)		
Rb(1)–S(1) (× 3)	3.199(2)	Rb(3)–S(4) (× 3)		3.452(2)
Rb(1)–S(2) (× 3)	3.519(1)	Rb(3)–S(5) (× 3)		3.508(2)
Rb(1)–S(3) (× 3)	3.817(2)	Rb(3)–S(5) (× 3)		4.054(2)
Rb(1)–S(t2)	3.214(3)	Rb(3)–S(t1)		3.433(3)
Rb(2)–S(3) (× 3)	3.664(2)			
Rb(2)–S(4) (× 3)	3.451(2)			
Rb(2)–S(5) (× 3)	3.649(2)			
		4 ($Rb_8Mo_{33}S_{37}$)		
Rb(1)–S(1) (× 3)	3.187(3)	Rb(3)–S(5) (× 3)		3.715(5)
Rb(1)–S(2) (× 3)	3.485(3)	Rb(3)–S(6) (× 3)		3.604(4)
Rb(1)–S(3) (× 3)	3.831(5)	Rb(3)–S(6) (× 3)		3.488(5)
Rb(1)–S(t2)	3.210(6)			
		Rb(4)–S(4) (× 3)		3.422(4)
Rb(2)–S(3) (× 3)	3.568(5)	Rb(4)–S(5) (× 3)		3.516(4)
Rb(2)–S(4) (× 3)	3.438(5)	Rb(4)–S(6) (× 3)		4.004(6)
Rb(2)–S(5) (× 3)	3.683(5)	Rb(4)–S(t1)		3.462(6)

RESULTS AND DISCUSSION

Descriptions of the Crystal Structures

Figure 1 shows the projections of the crystal structures of the different members onto the hexagonal (110) plane. The Mo–S networks of the $Rb_{2n}(Mo_9S_{11})(Mo_{6n}S_{6n+2})$ compounds are based on mixtures of Mo_9S_{11} and $Mo_{6n}S_{6n+2}$ ($n = 1$ to 4) cluster units (Fig. 2) which cocrystallize in equal proportion. The Mo_9 and Mo_{6n} cores result from the uniaxial trans-face-sharing of 2 and $2n$-1 octahedral Mo_6 clusters, respectively. While the structures of the first two members $Rb_2Mo_{15}S_{19}$ and $Rb_4Mo_{21}S_{25}$ belong to the structure types $In_2Mo_{15}Se_{19}$ (2) and $Cs_4Mo_{21}S_{25}$ (26) previously described, the structures of the other members are unprecedented. Figure 1 also shows clearly that the crystal structures of the new compounds derive from those of $Rb_2Mo_{15}S_{19}$ and $Rb_4Mo_{21}S_{25}$ by merely replacing the

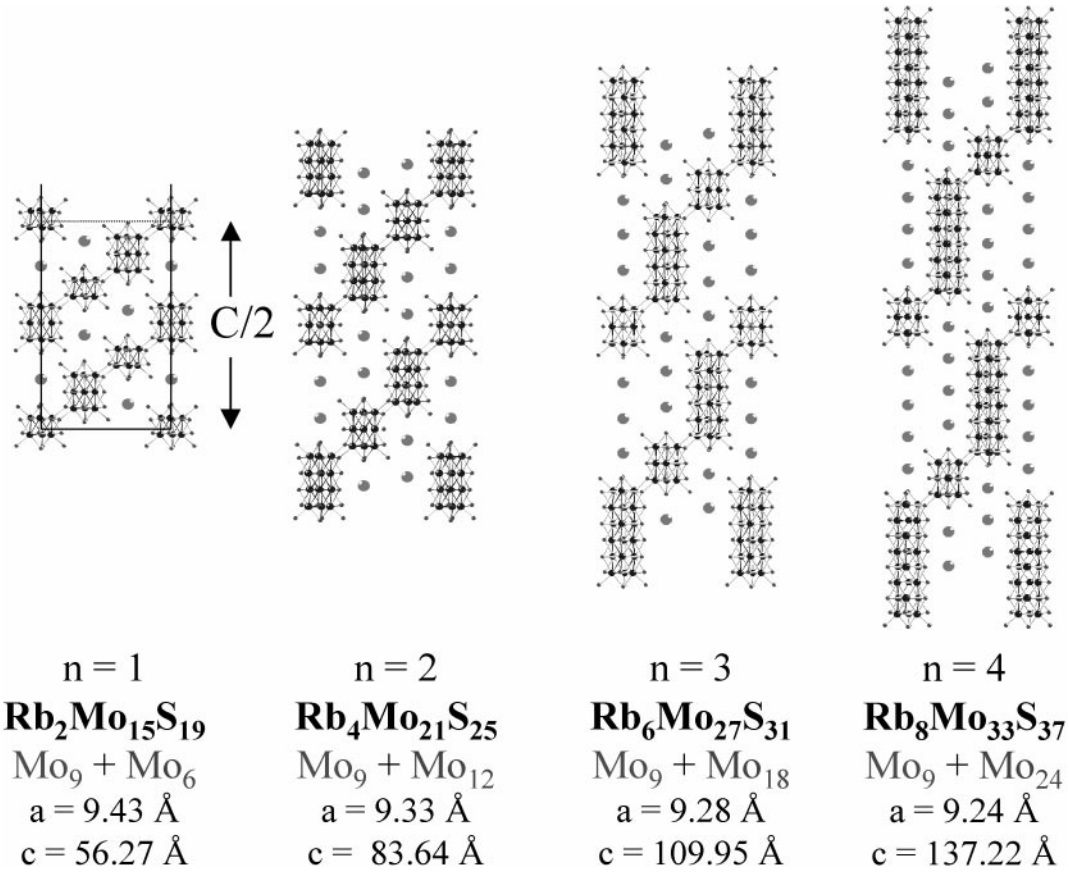

FIG. 1. Arrangement of the Mo_9S_{11} and $Mo_{6n}S_{6n+2}$ units ($n = 1$ to 4) and alkaline cations on the [110] plane in the $Rb_{2n}(Mo_9S_{11})(Mo_{6n}S_{6n+2})$ structure (intercluster distances have been omitted for clarity) (97% probability ellipsoids). For clarity, only half of the hexagonal unit cells along c are shown.

Mo_6 and Mo_{12} clusters by a larger even-membered Mo_{18} or Mo_{24} cluster, and inserting supplementary alkali metal cations in the larger voids resulting from the lengthening of the Mo_{6n} clusters. The structural evolution is reflected by the c parameter that increases linearly from 56.3 to 137.3 Å when n goes from 1 to 4, while the a parameter decreases from 9.43 to 9.23 Å in the hexagonal unit cell (Fig. 3). Regarding the rhombohedral lattice parameters, we observe a lengthening of the a parameter and a diminution of the rhombohedral α angle when n increases. This evolution is

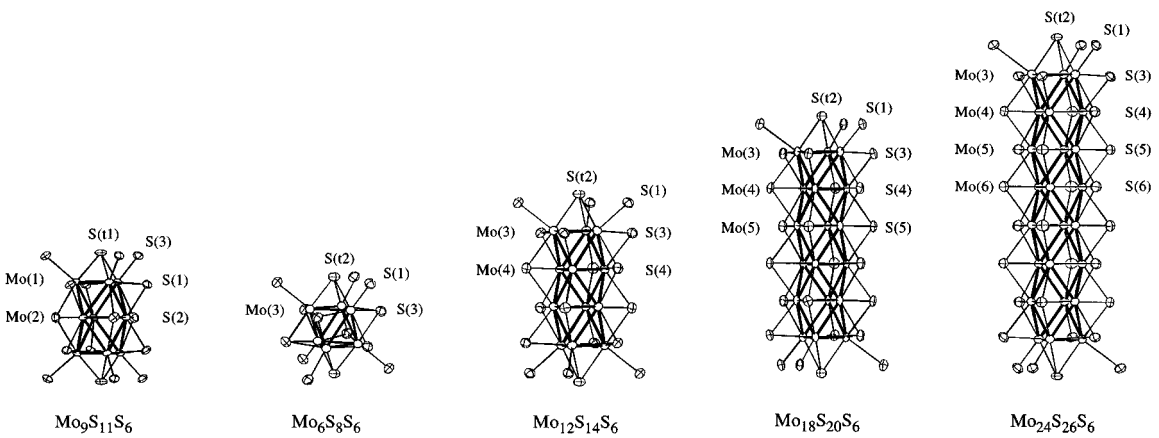

FIG. 2. Mo_9S_{11} and $Mo_{6n}S_{6n+2}$ cluster units ($n = 1$ to 4) with their sulfur environment.

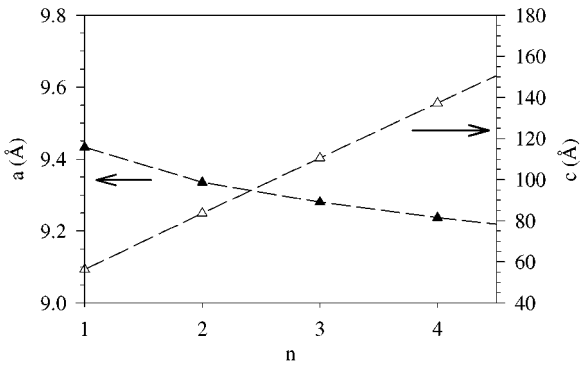

FIG. 3. Variation of the *a* and *b* lattice parameters of the hexagonal cell as a function of *n* in the $Rb_{2n}(Mo_9S_{11})(Mo_{6n}S_{6n+2})$ series.

also particularly well illustrated by the crystal shape of the different $Rb_{2n}(Mo_9S_{11})(Mo_{6n}S_{6n+2})$ compounds (Fig. 4).

The Mo_9S_{11} and $Mo_{6n}S_{6n+2}$ units are centered at 6*a* (D_3 or 32 symmetry) and 6*b* positions (S_6 or -3 symmetry), respectively. In both types of units, we can distinguish two kinds of Mo atoms: the inner and the outer. The inner Mo atoms are linked to six Mo atoms and four S atoms. The outer atoms are linked to four Mo atoms and five S atoms in a chalcogen square-based pyramidal coordination. Sulfur atoms of neighboring units occupy the apex of the pyramid. The Mo–Mo distances within the Mo_9 cluster are similar in the four members and vary between 2.666(2) and 2.688(3) Å for the intratriangle distances (distances within the Mo_3 triangles formed by the Mo atoms related through the three-fold axis) and between 2.719(1) and 2.7864(4) Å for those between the Mo_3 triangles (intertriangle distances). The average Mo–Mo distances within the Mo_9 clusters in the four members are quite homogeneous and only vary between 2.720 and 2.723 Å. This clearly shows that the number of electrons per Mo_9 cluster should be almost the same in the four structural types. For the $Mo_{6n}S_{6n+2}$ units, the intratriangle Mo–Mo distances range from 2.623(4) to 2.6868(7) Å and the intertriangle ones from 2.6573(4) to 2.767(2) Å. The average Mo–Mo distances are 2.722, 2.695, 2.684, and 2.681 Å when *n* goes from 1 to 4, indicating that the number of electrons per Mo atom increases when the cluster size augments. The sulfur atoms bridge either one [S(1), S(3), S(t1), and S(t2)] or two [S(2), S(4), S(5), and S(6)]

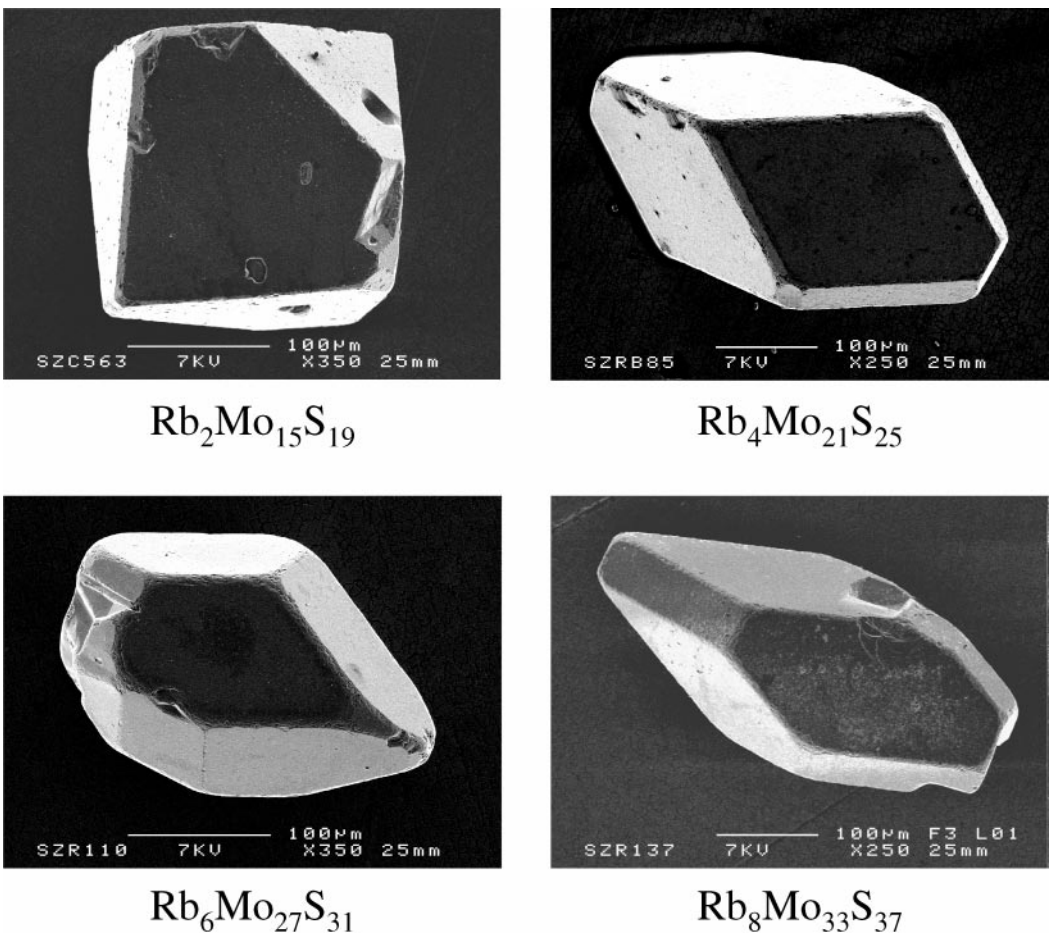

FIG. 4. Single-crystal photos of the different $Rb_{2n}(Mo_9S_{11})$ $(Mo_{6n}S_{6n+2})$ compounds ($n = 1$ to 4).

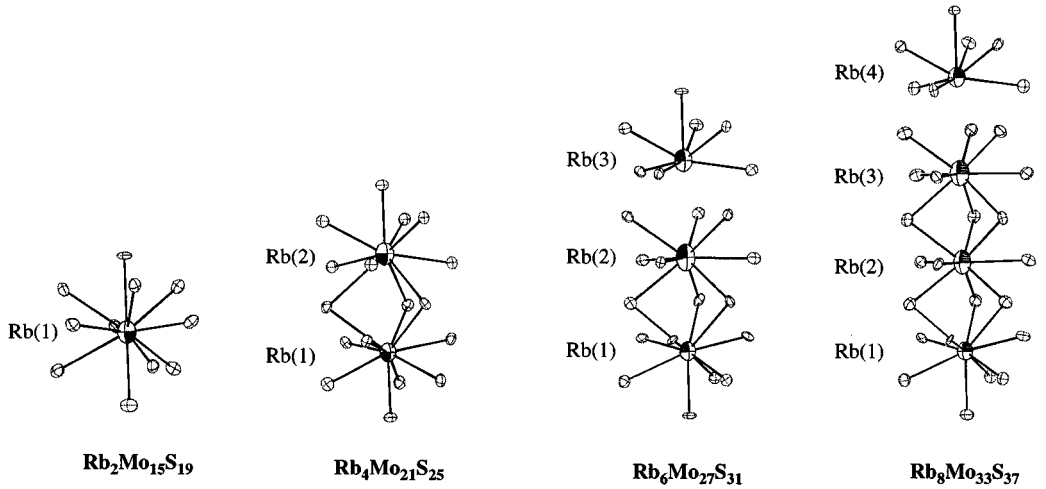

FIG. 5. Sulfur coordination around the Rb^+ ion sites for the $Rb_{2n}(Mo_9S_{11})(Mo_{6n}S_{6n+2})$ compounds ($n = 1$ to 4).

Mo triangular faces of the clusters. Moreover, the S(1) and S(3) atoms are linked to a Mo atom of a neighboring cluster. The Mo–S bond distances range from 2.416(3) to 2.624(2) Å within the Mo_9S_{11} unit and from 2.395(3) to 2.580(2) Å within the $Mo_{6n}S_{6n+2}$ units. Each Mo_9S_{11} unit is interconnected to six $Mo_{6n}S_{6n+2}$ units (and vice versa) via Mo(1)–S(3) bonds (respectively Mo(3)–S(1)) to form the three-dimensional Mo–S framework, the connective formula of which is $[Mo_9S^i_5S^{i-a}_{6/2}S^{a-i}_{6/2}][Mo_{6n}S^i_{6n-4}S^{i-a}_{6/2}S^{a-i}_{6/2}]$ in Schäfer's notation (27). From this arrangement, the shortest intercluster Mo(1)–Mo(3) distances between the Mo_9 and Mo_{6n} clusters are in the range 3.212–3.246 Å, indicating only a weak metal–metal interaction (vide infra).

The alkali metal cations are arranged in finite chains along the three-fold axis between two consecutive Mo_9S_{11} and $Mo_{6n}S_{6n+2}$ units in the distorted tri-, tetra-, or pentacapped trigonal prismatic environment of sulfur atoms (Fig. 5). The last environment is observed only in $Rb_2Mo_{15}S_{19}$ corresponding to the first member of the series. For the other members, the cations at both ends of the finite chain are in the tetracapped trigonal prismatic arrangement, and the remaining ones are in the tricapped trigonal coordination. The latter environment is similar to that encountered in the quasi-one-dimensional compounds $M_2Mo_6X_6$ (2). The Rb–S distances spread over a wide range, 3.187–4.054 Å. The spacing between adjacent Rb^+ cations lies between 4.520–4.903 Å.

Electronic Structure

Molecular and tight-binding extended Hückel calculations were performed on each member of the title family, using the experimental crystal structures. Very similar conclusions were obtained for all of them. Therefore, in this paper, only the electronic structure of the second member of the family, namely $Rb_4Mo_{21}S_{25}$, is analyzed. The total and projected densities of states (DOS) of $Rb_4Mo_{21}S_{25}$ are shown in the middle of Fig. 6. The molecular orbital (MO) diagrams of the isolated $[Mo_9S_{11}]^{2-}$ and $[Mo_{12}S_{14}]^{2-}$ clusters are given on each side of Fig. 6. The -2 charges given to these clusters are formal. Indeed, within a Zintl-type approach, only their sum has to be equal to -4 in order to balance the formal cationic charges. However, electron transfer between the clusters in the crystal can occur, which should lead to noninteger cluster charges. Moreover, due to the diffuse character of the orbitals of rubidium, some significant covalent interaction between the rubidium cations and the anionic cluster network is also expected, which would result in some anion → cation charge transfer. As a matter of fact, the calculated balance of charges in $Rb_4Mo_{21}S_{25}$ is $[Rb^{+0.82}]_4\ [Mo_9S_{11}]^{-1.19}\ [Mo_{12}S_{14}]^{-2.10}$.

For both isolated clusters, the overall distribution of the energy levels shows a rough separation of the chalcogen *p* states, lying lower in energy, and Mo *d* states which are situated closer (above and below) to the highest occupied MOs. A significant energy gap separates the bonding and antibonding Mo *d* states. Compared to results obtained with related selenium clusters (4), the metallic character of the highest occupied MOs is reinforced in the sulfur species, as expected from the energy difference between the valence atomic orbitals of S and Se (the 4*p* shell of the selenium lies at significantly higher energy than the 3*p* shell of the sulfur).

From our cluster MO diagrams and as noted previously by R. Gautier *et al.* for the related Mo_9Se_{11} and $Mo_{12}Se_{14}$ species (28), the closed-shell requirement would be satisfied if the 5*e* level of the Mo_9 cluster were fully occupied, as well as the 8*e* and $2a_2$ levels of the Mo_{12} cluster. This would lead to a stable situation in which the fully occupied bonding and nonbonding MOs would be separated from the empty

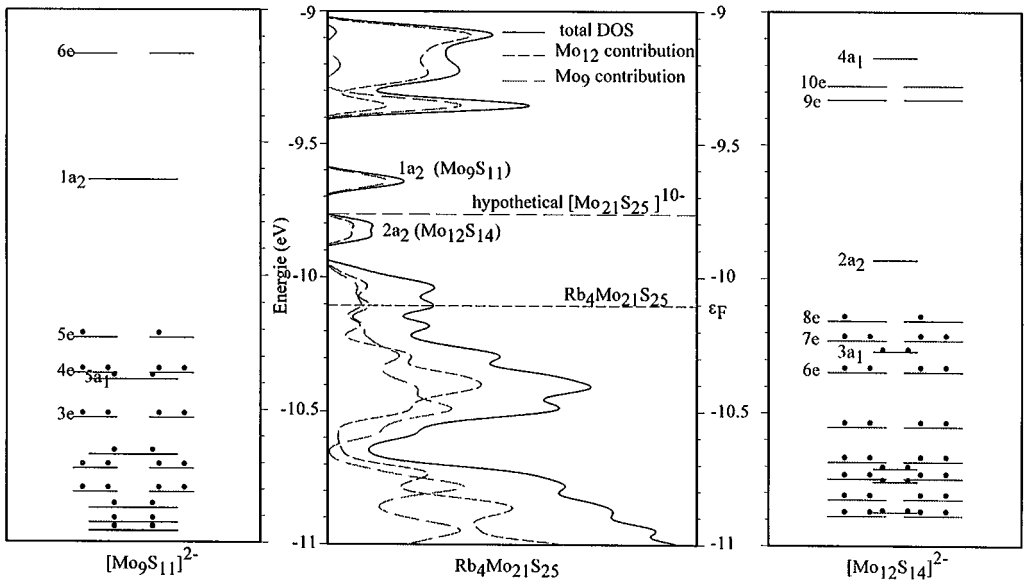

FIG. 6. Center: Total DOS (solid line), and its Mo_9 and Mo_{12} contributions in $Rb_4Mo_{21}S_{25}$. Left: MO diagrams of the isolated $[Mo_9S_{11}]^{2-}$ species. Right: MO diagrams of the isolated $[Mo_{12}S_{14}]^{2-}$ species. The -2 charges assigned to the isolated clusters are formal (see text).

antibonding ones. This would correspond to the hypothetical $[Mo_9S_{11}]^{4-}$ and $[Mo_{12}S_{14}]^{6-}$ species. Assuming an oxidation state of -2 for sulfur, the number of metallic electrons (MEs) is 36 for $[Mo_9S_{11}]^{4-}$ and 50 for $[Mo_{12}S_{14}]^{6-}$. The calculated cluster charges indicate that, in $Rb_4Mo_{21}S_{25}$, the $[Mo_9S_{11}]^{-1.19}[Mo_{12}S_{14}]^{-2.10}$ clusters are electron deficient with respect to the stability closed-shell requirement. This is a typical situation for this kind of compound (28, 29).

In the $Rb_4Mo_{21}S_{25}$ solid, the Mo_9S_{11} and $Mo_{12}S_{14}$ units interact mainly via Mo–S bonds, and also to some extent via Mo–Mo contacts. The making of the former tends to somewhat destabilize the Mo-based orbitals of the clusters. Each individual MO of the isolated clusters gives rise to a rather narrow band. Bands generated by levels which are close in energy overlap, leading to the DOS displayed in the middle of Fig. 6. The states which are situated above and below the Fermi level are generated by the 5*e* and 8*e* HOMOs of $[Mo_9S_{11}]^{2-}$ and $[Mo_{12}S_{14}]^{2-}$, respectively, in a close to 50:50 ratio (Fig. 6). The first unoccupied band derives from the nonbonding $2a_2$ MO of $Mo_{12}S_{14}$, whereas the second one derives from the antibonding $1a_2$ MO of Mo_9S_{11}. The occupation of all the states up to the top of the $2a_2$ ($Mo_{12}S_{14}$) band should be possible without modifying drastically the Mo–S and Mo–Mo frameworks. This would correspond to the $[Mo_9S_{11}]^{4-}$ and $[Mo_{12}S_{14}]^{6-}$ cluster oxidation states, *i.e.*, to the satisfaction of the closed-shell requirement, associated with a semiconducting behavior. Experimental work on related Se compounds has shown that it is possible to reduce them, at least to some extent, by inserting transition metals in the empty voids of the crystal (28).

Examination of the Mo–Mo separations in the crystal suggests significant metal–metal bonding within the clusters and weak metal–metal bonding between the clusters (see above). The average calculated Mo–Mo overlap populations are 0.245 (intracluster) and 0.061 (intercluster). This latter value is indicative of a rather weak, but significant, bonding interaction. Thus, some metallic behavior is expected from the calculations for $Rb_4Mo_{21}S_{25}$.

Resistivity Properties

Electrical resistivity measurements performed on different single crystals of each member of the family $Rb_{2n}(Mo_9S_{11})(Mo_{6n}S_{6n+2})$ ($n = 1$ to 4) indicated that they are poorly metallic, with room temperature resistivity around 1 mΩ.cm, and become superconductors with critical temperatures ranging from 4.2 K to 10.9 K (see Table 4). Superconductivity was also confirmed by the Meissner effect from dc susceptibility measurements on powder samples for the four compounds investigated. For each single crystal

TABLE 4
Critical Superconducting Temperature of $Rb_{2n}(Mo_9S_{11})(Mo_{6n}S_{6n+2})$ Compounds ($n = 1$ to 4)

	$Rb_2Mo_{15}S_{19}$	$Rb_4Mo_{21}S_{25}$	$Rb_6Mo_{27}S_{31}$	$Rb_8Mo_{33}S_{37}$
T_c	4.2 K	11 K	7 K	5.8 K

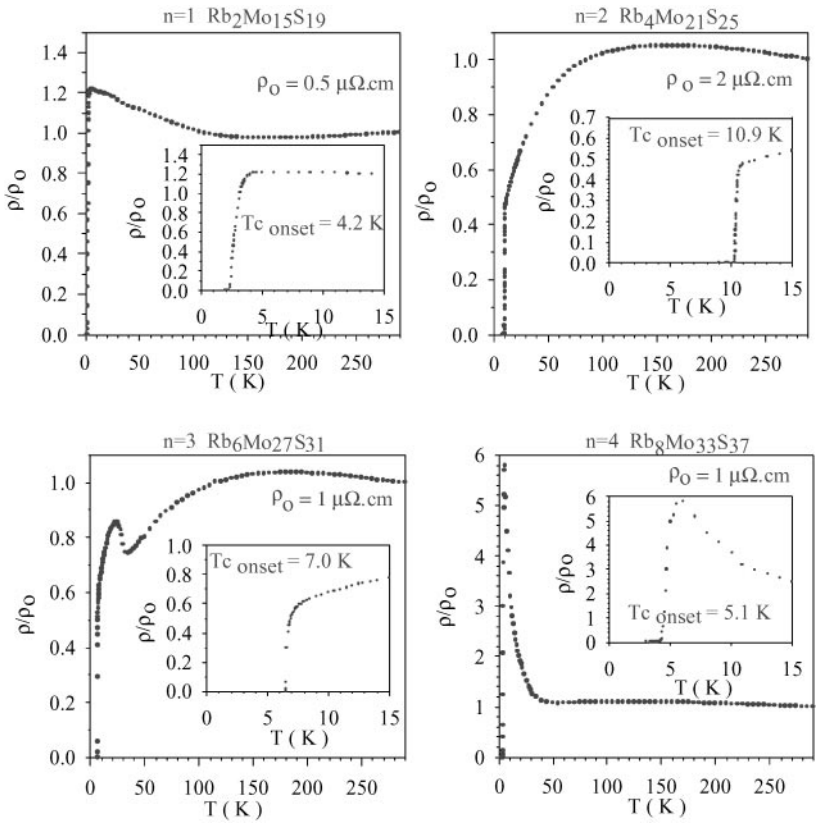

FIG. 7. Temperature dependencies of the resistivity of $Rb_{2n}(Mo_9S_{11})$ $(Mo_{6n}S_{6n+2})$ ($n = 1$ to 4) single crystals. Critical superconducting transition is given in the inset.

studied, the current was applied in the c direction of the hexagonal unit cell. Figure 7 illustrates the unusual temperature dependence of the resistivity for each member. For the second and the third compounds, a small increase of the resistivity from room temperature to a maximum at approximately 120 K is observed, and then a decrease occurs which is followed for the third member by a new increase of the resistivity just before the superconducting transition which is generally 1 K broad (inserts Fig. 7). For the fourth member, a very slight increase of the resistivity is observed from room temperature to 40 K, followed by a strong increase ($\rho_{6K}/\rho_{RT} \approx 6$) just before the superconducting transition at 5.1 K. Similar resistivity curves have been observed previously for other ternary molybdenum chalcogenides containing condensed clusters (14). Such behaviors are typical of materials near a metal–insulator boundary. The upper critical fields parallel and perpendicular to the cluster elongation axis were determined on a single crystal of $Rb_6Mo_{27}S_{31}$ by monitoring the resistive transitions induced by the magnetic field. We have plotted in Fig. 8 the resistive transitions observed at five different temperatures for the two orientations of the applied magnetic field (parallel (solid lines) and perpendicular (dashed line) to the c axis of the hexagonal unit cell). As in the previous experiments, the current was applied in the c direction. From these curves, we could plot the critical fields $Hc_{2//}$ and $Hc_{2\perp}$ as a function of the temperature as shown in Fig. 9. By linear extrapolation, $Hc_{2//}$ and $Hc_{2\perp}$ were estimated to be 31 T and 28 T at 0 K, respectively.

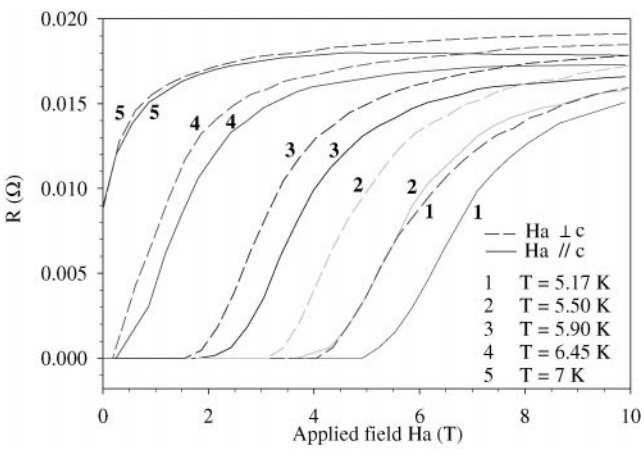

FIG. 8. Resistive transitions of $Rb_6Mo_{27}S_{31}$ ($n = 3$) as a function of the magnetic field for a polar angle of 0° (—) and 90° (- - -) at different temperatures.

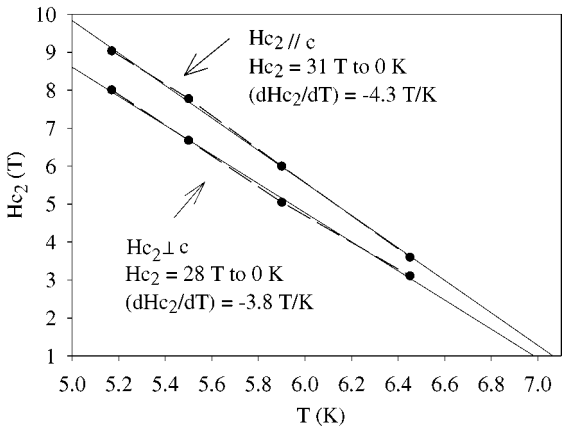

FIG. 9. Variation of the critical fields $Hc_{2//}$ and $Hc_{2\perp}$ of $Rb_6Mo_{27}S_{31}$ as a function of the temperature.

The latter values are between those determined for $PbMo_6S_8$ ($Hc_{2\perp} = 70$ T) and $Cs_2Mo_{12}Se_{14}$ ($Hc_{2//} = 12.7$ T and $Hc_{2\perp} = 30$ T) (14). The initial slopes dHc_2/dT were found to be close to -4 T/K ($dHc_{2\perp}/dT = -3.8$ and $dHc_{2//}/dT = -4.3$ T/K).

CONCLUDING REMARKS

This study has allowed four new rubidium-reduced molybdenum sulfides to be synthesized. These compounds form an original new family with general formula $Rb_{2n}(Mo_9S_{11})(Mo_{6n}S_{6n+2})$ ($n = 1$ to 4). Their crystal structures are characterized by a mixture of Mo_9S_{11} and $Mo_{6n}S_{6n+2}$ ($n = 1$ to 4) cluster units in equal proportions separated by large voids in which the rubidium cations reside. Electrical resistivity measurements carried out on single crystals showed that the four members are superconducting with critical temperatures ranging from 4.2 K to 10.9 K. An interesting feature of their electrical behavior is the upturn of the resistivity just before the superconducting transition that increases with n. This clearly shows that the $Rb_{2n}(Mo_9S_{11})(Mo_{6n}S_{6n+2})$ compounds are near a metal–insulator boundary. Finally, it should be mentioned that the existence of larger even-membered Mo_{30} and Mo_{36} clusters in $Cs_8Mo_{30}S_{32}$ and $Rb_{10}Mo_{36}S_{38}$ suggest that members of the $Rb_{2n}(Mo_9S_{11})(Mo_{6n}S_{6n+2})$ series with $n = 5$ and 6 should exist.

ACKNOWLEDGMENTS

S.P. thanks Dr. P. Monceau (C.R.T.B.T.—Grenoble) for receiving her in his laboratory for the resistivity measurements under magnetic field and for helpful discussions.

REFERENCES

1. A. Grüttner, K. Yvon, R. Chevrel, M. Potel, M. Sergent, and B. Seeber, *Acta Crystallogr. B* **35,** 285 (1979).
2. M. Potel, R. Chevrel, and M. Sergent, *Acta Crystallogr. B* **37,** 1007 (1981).
3. R. Chevrel, M. Potel, M. Sergent, M. Decroux, and Ø. Fischer, *Mater. Res. Bull.* **15,** 867 (1980).
4. P. Gougeon, J. Padiou, J.-Y. Le Marouille, M. Potel, and M. Sergent, *J. Solid State Chem.* **51**, 218 (1984); S. Picard, J.-F. Halet, P. Gougeon, and M. Potel, *Inorg. Chem.* **38,** 4422–4429 (1999).
5. P. Gougeon, M. Potel, J. Padiou, and M. Sergent, *Mater. Res. Bull.* **22,** 1087 (1988); C. Thomas, S. Picard, R. Gautier, P. Gougeon, and M. Potel, *J. Alloys Compd.* **262–263,** 305–310 (1997); R. Gautier, S. Picard, P. Gougeon, and M. Potel, *Mater. Res. Bull.* **34,** 93–101 (1999).
6. P. Gougeon, M. Potel, and M. Sergent, *Acta Crystallogr. C* **45,** 182 (1989); P. Gougeon, M. Potel, and M. Sergent, *Acta Crystallogr. C* **45,** 1413 (1989).
7. P. Gougeon, M. Potel, J. Padiou, and M. Sergent, *Mater. Res. Bull.* **23,** 453 (1988).
8. P. Gougeon, M. Potel, and M. Sergent, *Acta Crystallogr. C* **46,** 2284 (1990); S. Picard, P. Gougeon, and M. Potel, *Acta Crystallogr. C* **53,** 1519 (1997).
9. S. Picard, M. Potel, and P. Gougeon, *Angew. Chem.* **38,** 2023 (1999).
10. P. Gougeon, Thesis, Rennes, 1984.
11. R. Chevrel and M. Sergent, *in* "Superconducting in Ternary Compounds," (Ø. Fischer and M. B. Maple, Eds.) Part I, Springer Verlag, Berlin, Heidelberg, New York, 1982.
12. M. Potel, Thesis, Rennes, 1984.
13. P. Gougeon, M. Potel, J. Padiou, and M. Sergent, *J. Solid State Chem.* **68,** 137 (1987).
14. R. Brusetti, O. Laborde, A. Sulpice, R. Calemczuk, M. Potel, and P. Gougeon, *Phys. Rev. B* **52,** 4481 (1995)
15. J. C. Armici, M. Decroux, Ø. Fischer, M. Potel, R. Chevrel, and M. Sergent, *Solid State Commun.* **33,** 607 (1980).
16. R. Lepetit, P. Monceau, M. Potel, P. Gougeon, and M. Sergent, *J. Low Temp. Phys.* **56,** 219 (1984).
17. R. Brusetti, P. Monceau, M. Potel, P. Gougeon, and M. Sergent, *Solid State Commun.* **66,** 181 (1988).
18. R. Brusetti, A. Briggs, O. Laborde, M. Potel, and P. Gougeon, *Phys. Rev. B* **49,** 8931 (1994).
19. A. C. T. North, D. C. Phillips, and F. S. Mathews, *Acta Crystallogr. A* **24,** 351 (1968).
20. C. K. Fair, "MolEN User's Manual. An Interactive Intelligent System For Crystal Structure Analysis." Enraf-Nonius, Delft, The Netherlands, 1989.
21. V. Petricek, JANA98: Crystallographic Computing Cystem for Ordinary and Modulated Structures, 1998.
22. R. Hoffmann, *J. Chem. Phys.* **39,** 1397 (1963).
23. M. H. Whangbo, and R. Hoffmann, *J. Am. Chem. Soc.* **100,** 6093 (1978).
24. C. Mealli and D. Proserpio, *J. Chem. Educ.* **67,** 399 (1990).
25. G. A. Landrum, YAeHMOP Yet Another Extended Hückel Molecular Orbital Package, version 2.0, Ithaca, NY, 1997.
26. P. Gougeon and M. Potel, *Acta Crystallogr. C* **49,** 427 (1993).
27. H. Shäfer and H. G. Von Schnering, *Angew. Chem.* **20,** 833 (1964).
28. R. Gautier, P. Gougeon, J. F. Halet, M. Potel, and J. Y. Saillard, *J. Alloys Compd.* **262,** 311 (1997).
29. A Simon, *in* "Metal Clusters and Colloids" (G. Schmid, Ed.), p. 373. Weinheim, Verlag.